MODE EXPANSION SOLUTION FOR SCATTERING BY A MATERIAL FILLED RECTANGULAR GROOVE

M. A. Morgan

Electrical and Computer Engineering Department
Naval Postgraduate School
833 Dyer Road, Room 437
Monterey, CA 93943, USA

F. K. Schwering

Space and Terrestrial Communication Directorate
ATTN: AMSEL-RD-ST
Fort Monmouth, NJ 07703, USA

1. CONCEPT

The solution of scattering by a 2-D trough in an infinite conducting ground plane may be formulated using any of several approaches, including integral equations [1], impedance boundary conditions [2–3], finite elements [4], Fourier transforms [5–6] and cavity mode coupling to exterior region cylindrical harmonics [7]. An efficient technique requiring no matrix inversions nor special function evaluations is developed here for the case of a rectangular groove containing homogeneous, perhaps lossy, isotropic material.

The 2-D scattering geometry is shown in Fig. 1(a), with a rectangular cavity of width W and depth d in an infinite, perfect electric

conductor (pec) ground plane. Incident plane wave fields both TM to z (E-Pol) and TE to z (H-Pol) are considered. Material within the groove has relative constituent parameters ϵ_{r1} and μ_{r1}, either or both of which may be complex under lossy conditions. Scattered fields in the half-space above the groove are defined as $\overline{E}^S = \overline{E}_1 - \overline{E}_2$ and $\overline{H}^S = \overline{H}_1 - \overline{H}_2$ where $(\overline{E}_1, \overline{H}_1)$ are the total fields in the presence of the ground plane containing the groove and $(\overline{E}_2, \overline{H}_2)$ are the total fields with the infinite ground plane present without the groove.

An exact equivalence for scattering by an open cavity in a ground plane having any shape and material filling is developed in the Appendix. According to this equivalence, the previously defined scattered field is generated by an impressed surface current, $-\overline{J}_S(x) = -2\hat{y} \times \overline{H}_i(x,0)$, placed over the cavity aperture. The fields produced within the cavity by this equivalent current are the same as those due to the original incident field. It should be noted that this form of equivalence is different than the magnetic current approach used to derive cavity aperture integral equations.

To formulate the equivalent problem solution, we decompose the cavity fields into combinations of parallel plate waveguide modes (forming cavity modes) and evaluate the coupling into each such mode by the impressed $-\overline{J}_S(x)$ driving the aperture in place of the original incident field. Once the cavity mode coefficients are found, the far-zone scattered fields and 2-D radar cross section (RCS) per unit length (also referred to as *scattering width*), are evaluated using Green's function integrations of $\overline{E}_{\text{tan}}$ modal expansions over the aperture.

A rigorous solution to mode coupling in such a formulation requires enforcement of correct radiation field behavior in the upper half-space. This can be accomplished by using: (1) an integral equation; (2) a terminated finite element mess, or; (3) coupling to a radially propagating cylindrical harmonic expansion.

The mode coupling solution can be simplified by expanding the field in the local region above the aperture using upward propagating waveguide modes bounded by vertical walls, as illustrated in Fig. 1(b). These modes satisfy Maxwell's equations, are outbound from the aperture, and provide a basis for expansion of the local field. Such an approach allows simple mode-by-mode field matching across the aperture without the need for matrix inversion. This provides a very rapid solution, even for electrically large apertures.

(a)

(b)
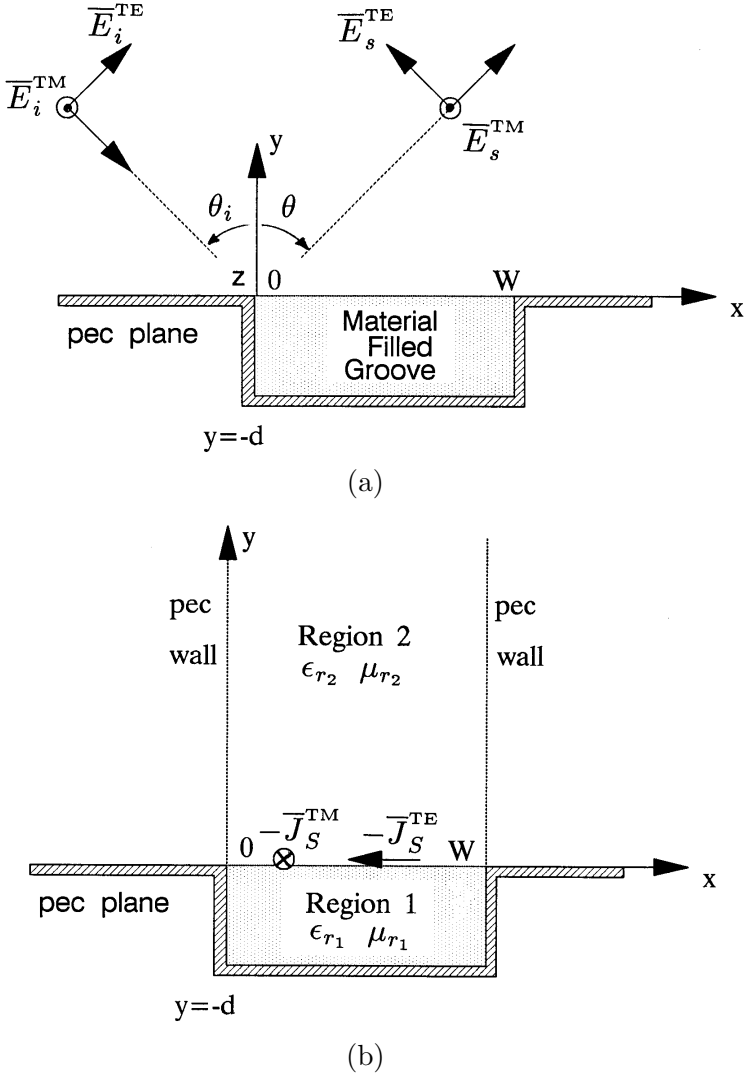
Figure 1. Scattering by a Material Filled Rectangular Groove in a PEC Ground Plane: (a) Original Configuration with Incident Field; (b) Approximation with Equivalent Current and Artificial Waveguide Walls in Upper Half-Space.

However, replacing the upper half-space with a guided wave structure introduces a physical approximation which ignores interaction of the driving current $-\overline{J}_S(x)$ with the remainder of the ground plane

(including upper corners of the groove). Instead, interaction is considered with the vertical waveguide walls. Resultant TM case field expansions will not experience the field singularity near the upper corners. As will be demonstrated, for aperture dimensions exceeding about one wavelength the neglected effects usually produce only small perturbations to the scattered field, the generation of which tends to be dominated by interactions with the aperture and cavity of the groove.

2. FORMULATION

Fourier sine and cosine series are used to represent $\overline{J}_S(x) = 2\hat{y} \times \overline{H}_i(x,0)$ for respective TM and TE plane wave incident fields, each having amplitudes $|\overline{H}_i| = H_0$ and $|\overline{E}_i| = E_0 = \eta_0 H_0$, where $\eta_0 = 120\pi\Omega$. These series match the modal variations in x of the cavity and waveguide fields in Regions 1 and 2.

$$\overline{J}_S^{TM}(x) = 2H_0\hat{z}\cos\theta_i \; e^{-jk_0 x \sin\theta_i} \doteq H_0\hat{z}\sum_{n=1}^{N} a_n^{TM} \sin\left(\frac{n\pi}{W}x\right) \quad (1a)$$

$$\overline{J}_S^{TE}(x) = 2H_0\hat{x} \; e^{-jk_0 x \sin\theta_i} \doteq H_0\hat{x}\sum_{n=0}^{N} a_n^{TE} \cos\left(\frac{n\pi}{W}x\right) \qquad (1b)$$

Fourier sine and cosine series integrations yield

$$a_n^{TM} = [1 - (-1)^n \; e^{-jk_0 W \sin\theta_i}]\frac{2n\pi\cos\theta_i}{(n\pi)^2 - (k_0 W \sin\theta_i)^2} \quad \text{for} \quad n \geq 1 \tag{2a}$$

$$a_n^{TE} = [1 - (-1)^n \; e^{-jk_0 W \sin\theta_i}]\frac{j\varepsilon_n k_0 W \sin\theta_i}{(n\pi)^2 - (k_0 W \sin\theta_i)^2} \quad \text{for} \quad n \geq 0 \tag{2b}$$

with $\varepsilon_0 = 1$ and $\varepsilon_n = 2$ for $n \geq 1$.

Region 1 cavity modes are formed from pairs of $\pm y$ directed parallel plate waveguide modes [8] to satisfy $\overline{E}_{\tan}(x, -d) = 0$ on the groove bottom. Field components parallel to the aperture are given for $-d \leq y \leq 0$ by

$$E_z^{TM}(x, y) \doteq E_0 \sum_{n=1}^{N} b_n^{TM} \sin\left(\frac{n\pi}{W}x\right) \sinh[\gamma_n(y + d)] \qquad (3a)$$

$$H_x^{TM}(x,y) \doteq \frac{\jmath H_0}{k_0 \mu_{r1}} \sum_{n=1}^{N} b_n^{TM} \gamma_n \sin\left(\frac{n\pi}{W}x\right) \cosh[\gamma_n(y+d)] \quad (3b)$$

$$H_z^{TE}(x,y) \doteq H_0 \sum_{n=0}^{N} b_n^{TE} \cos\left(\frac{n\pi}{W}x\right) \cosh[\gamma_n(y+d)] \quad (3c)$$

$$E_x^{TE}(x,y) \doteq \frac{-\jmath E_0}{k_0 \epsilon_{r1}} \sum_{n=0}^{N} b_n^{TE} \gamma_n \cos\left(\frac{n\pi}{W}x\right) \sinh[\gamma_n(y+d)] \quad (3d)$$

where $\gamma_n = \sqrt{(n\pi)/W)^2 - k_0^2 \mu_{r1}\epsilon_{r1}}$.

Region 2 fields are expanded for $y \geq 0$ using $+y$ directed waveguide modes,

$$E_z^{TM}(x,y) \doteq E_0 \sum_{n=1}^{N} c_n^{TM} \sin\left(\frac{n\pi}{W}x\right) e^{-\nu_n y} \quad (4a)$$

$$H_x^{TM}(x,y) \doteq \frac{-\jmath H_0}{k_0 \mu_{r2}} \sum_{n=1}^{N} c_n^{TM} \nu_n \sin\left(\frac{n\pi}{W}x\right) e^{-\nu_n y} \quad (4b)$$

$$H_z^{TE}(x,y) \doteq H_0 \sum_{n=0}^{N} c_n^{TE} \cos\left(\frac{n\pi}{W}x\right) e^{-\nu_n y} \quad (4c)$$

$$E_x^{TE}(x,y) \doteq \frac{\jmath E_0}{k_0 \epsilon_{r2}} \sum_{n=0}^{N} c_n^{TE} \nu_n \cos\left(\frac{n\pi}{W}x\right) e^{-\nu_n y} \quad (4d)$$

where $\nu_n = \sqrt{(n\pi/W)^2 - k_0^2 \mu_{r2}\epsilon_{r2}}$.

A small amount of loss may be introduced into Region 2 by using $\epsilon_{r2} = 1 - \jmath\epsilon_{r2}''$ and $\mu_{r2} = 1 - \jmath\mu_{r2}''$ to improve the solution accuracy when $W \approx M\lambda_0/2$, with M an integer. This loss acts to inhibit resonant standing waves produced by the artificial parallel plate waveguide section which bounds Region 2. Values of $\epsilon_{r2}'' = \mu_{r2}'' = 0.01$ are used in the validations of Section 3. For W not close to multiples of $\lambda_0/2$ this small loss has virtually no effect on the solution.

Field expansion coefficients are found by enforcing continuity conditions at the aperture boundary between Regions 1 and 2,

$$\lim_{\delta y \to 0^+} \hat{y} \times [\overline{H}(x,\delta y) - \overline{H}(x,-\delta y)] = -\overline{J}_S(x) \quad (5a)$$

$$\lim_{\delta y \to 0^+} \hat{y} \times [\overline{E}(x,\delta y) - \overline{E}(x,-\delta y)] = \overline{0} \quad (5b)$$

Mode-by-mode substitution from appropriate expansions in (1), (3), and (4) yields two linear equations for each pair of modal expansion coefficients, whose solutions are

$$c_n^{TM} = b_n^{TM} \sinh(\gamma_n d) = \frac{2\jmath k_0 \mu_{r1} \mu_{r2} \sinh(\gamma_n d)}{\mu_{r1} \nu_n \sinh(\gamma_n d) + \mu_{r2} \gamma_n \cosh(\gamma_n d)} a_n^{TM} \quad (6a)$$

and

$$c_n^{TE} = -\frac{\gamma_n \epsilon_{r2}}{\nu_n \epsilon_{r1}} b_n^{TE} \sinh(\gamma_n d) = \frac{-2\epsilon_{r2} \gamma_n \sinh(\gamma_n d)}{\epsilon_{r2} \gamma_n \sinh(\gamma_n d) + \epsilon_{r1} \nu_n \cosh(\gamma_n d)} a_n^{TE} \tag{6b}$$

With identical material in both regions, where $\epsilon_{r1} = \epsilon_{r2}$ and $\mu_{r1} = \mu_{r2}$, the above simplifies to $c_n^{TM} = \frac{\jmath k_0 \mu_{r1}}{\nu_n}[1 - \exp(-2\nu_n d)]a_n^{TM}$ and $c_n^{TE} = -[1 - \exp(-2\nu_n d)]a_n^{TE}$.

Far-zone scattered fields can now be evaluated using Green's function integrations of the tangential electric fields in the aperture [9] using

$$\overline{E}_S^{TM}(\rho, \theta) = \hat{z}\sqrt{\frac{\jmath k_0}{2\pi\rho}} \; e^{-\jmath k_0 \rho} \cos\theta \int_0^W E_z^{TM}(x,0) e^{\jmath k_0 x \sin\theta} dx \quad (7a)$$

$$\overline{H}_S^{TE}(\rho, \theta) = -\frac{\hat{z}}{\eta_0}\sqrt{\frac{\jmath k_0}{2\pi\rho}} \; e^{-\jmath k_0 \rho} \int_0^W E_x^{TE}(x,0) e^{\jmath k_0 x \sin\theta} dx \qquad (7b)$$

Substituting expansions for $E_z^{TM}(x,0)$ and $E_x^{TE}(x,0)$ into (7), using (4a) and (4d), gives

$$\overline{E}_S^{TM}(\rho, \theta) \doteq E_0 W \hat{z}\sqrt{\frac{\jmath k_0}{2\pi\rho}} \; e^{-\jmath k_0 \rho} \sum_{n=1}^{N} c_n^{TM} I_n(\theta) \qquad (8a)$$

$$\overline{H}_S^{TE}(\rho, \theta) \doteq H_0 W \hat{z}\sqrt{\frac{\jmath k_0}{2\pi\rho}} \; e^{-\jmath k_0 \rho} \sum_{n=0}^{N} c_n^{TE} L_n(\theta) \qquad (8b)$$

where $I_n(\theta)$ and $L_n(\theta)$ represent far-field Fourier integrations of modal aperture fields

$$I_n(\theta) = \frac{\cos\theta}{W} \int_0^W \sin\left(\frac{n\pi x}{W}\right) e^{\jmath k_0 x \sin\theta} dx$$

$$= [1 - (-1)^n e^{jk_0 W \sin\theta}] \frac{n\pi \cos\theta}{(n\pi)^2 - (k_0 W \sin\theta)^2} \quad (9a)$$

$$L_n(\theta) = \frac{-j\nu_n}{k_0 W \epsilon_{r2}} \int_0^W \cos\left(\frac{n\pi x}{W}\right) e^{jk_0 x \sin\theta} dx$$

$$= \frac{-\nu_n}{k_0 \epsilon_{r2}} [1 - (-1)^n e^{jk_0 W \sin\theta}] \frac{k_0 W \sin\theta}{(n\pi)^2 - (k_0 W \sin\theta)^2} \quad (9b)$$

Bistatic RCS is then computed using

$$\sigma^{TM}(\theta) = \lim_{\rho\to\infty} 2\pi\rho \frac{|\overline{E}_S^{TM}(\rho,\theta)|^2}{|E_0|^2} \doteq k_0 W^2 \left|\sum_{n=1}^N c_n^{TM} I_n(\theta)\right|^2 \quad (10a)$$

$$\sigma^{TE}(\theta) = \lim_{\rho\to\infty} 2\pi\rho \frac{|\overline{H}_S^{TE}(\rho,\theta)|^2}{|H_0|^2} \doteq k_0 W^2 \left|\sum_{n=0}^N c_n^{TE} L_n(\theta)\right|^2 \quad (10b)$$

For lossless media in the groove, the solution converges rapidly with increasing n for $n \geq 2\frac{W}{\lambda_0}\sqrt{\epsilon_{r1}\mu_{r1}}$, wherein evanescent modes are being encountered in Region 1. Using this as a guide for the general case, a series truncation of $N = 2\frac{W}{\lambda_0}\sqrt{|\epsilon_{r1}\mu_{r1}|}$ has provided excellent convergence for RCS under all conditions tested.

3. VALIDATIONS

Comparisons are made here with other published results in [2–6] and with direct computations performed using a multi-region cylindrical harmonic expansion formulation [7]. Since $f = 300$ MHz ($\lambda_0 = 1m$) in all computations, the 2-D RCS, given in dB-meters, can also be considered as wavelength normalized σ/λ_0, expressed dB.

Since no matrix inversions are required, computed time is extremely brisk. Bistatic scattering from a $W = 10.2m$ by $d = 16.0m$ groove for 91 incident angles and 181 scattering angles requires only 3.0 seconds (with 20.7 Mflops) to compute using MatLab 4.2 on a 90MHz Pentium personal computer.

Figure 2 displays TE case bistatic RCS when $\theta_i = 60°$ for a rectangular groove with $W = 2m$ and $d = 0.5m$, filled with lossy material having $\epsilon_r = 2.5 - j0.2$ and $\mu_r = 1.8 - j0.1$. RCS computed using the waveguide mode (WGM) method and an aperture integral equation solution given in [2] are overlaid. The WGM approach provides good overall accuracy, with increasing dB errors appearing only at low relative values
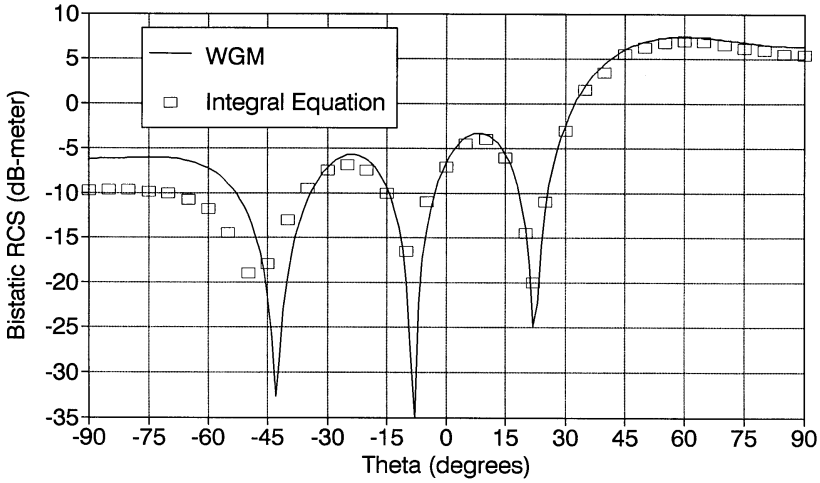
Figure 2. Bistatic 2-D RCS for TE Incidence at $\theta_i = 60°$ on a Groove with $W = 2m$, $d = 0.5m$, $\epsilon_r = 2.5 - \jmath 0.2$ and $\mu_r = 1.8 - \jmath 0.1$. Comparing calculations using Waveguide Modes (WGM) to that from an Integral Equation in [2] at $f = 300$ MHz.
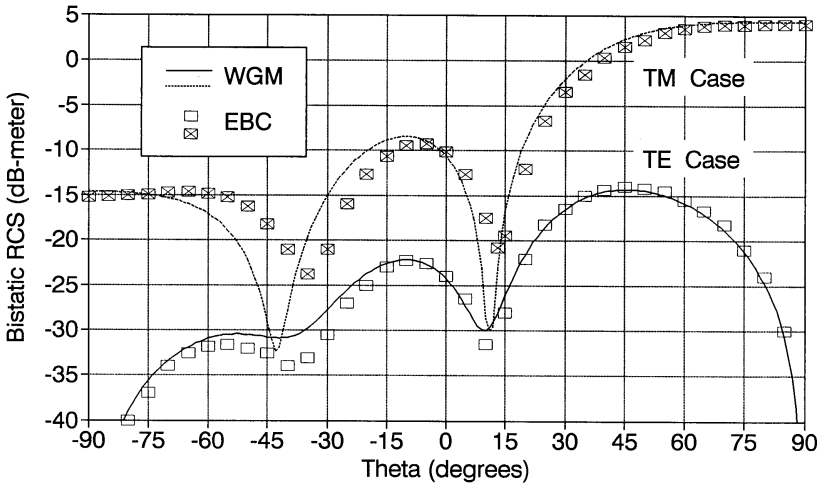
Figure 3. Bistatic 2-D RCS for Near Grazing Incidence at $\theta_i = 80°$ on a Shallow Groove with $W = 1.25m$, $d = 0.0625m$, $\epsilon_r = 16 - \jmath 5$ and $\mu_r = 4 - \jmath 1.25$. Comparing TE and TM Case computations using Waveguide Modes (WGM) to those using the "Exact Boundary Condition" (EBC) solution in [3] at $f = 300$ MHz.
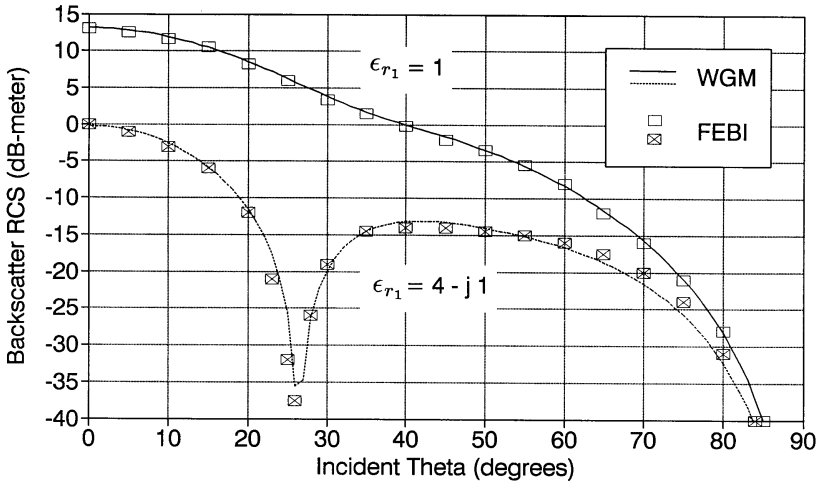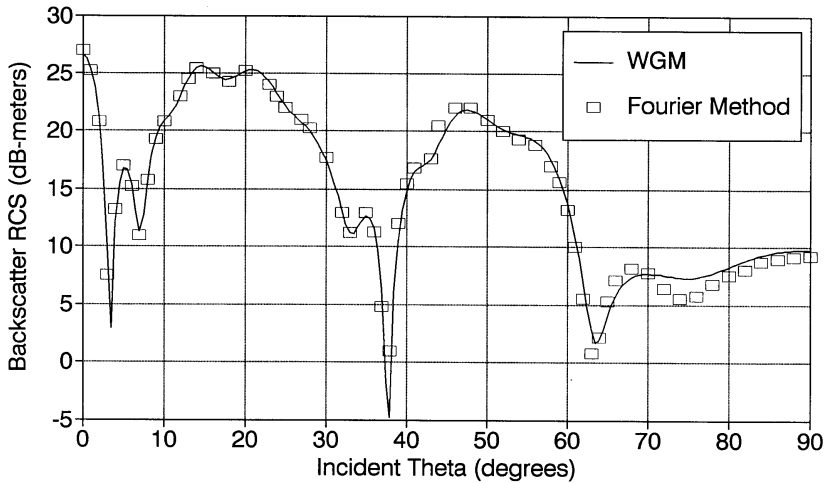
Figure 4. Backscattering 2-D RCS for TM Incidence on a Rectangular Groove with $W = 1.0m$ and $d = 0.25m$. Comparing calculations using Waveguide Modes (WGM) to those from a Finite Element Boundary Integral (FEBI) Approach in [4] at $f = 300$ MHz for two cases: $\epsilon_r = 1$ (vacuum) and $\epsilon_r = 4 - j1$ (lossy dielectric).

Bistatic RCS is also compared in Fig. 3 for the case of near-grazing ($\theta_i = 80°$) TE and TM incidence on a shallow rectangular groove with $W = 1.25m$ and $d = .0625m$. The groove is filled with dense lossy material having $\epsilon_r = 16 - j5$ and $\mu_r = 4 - j1.25$. The WGM approach provides good agreement with an "exact boundary condition" (EBC) method developed in [3].

Figure 4 overlays backscattered RCS for TM incidence on a rectangular groove having $W = 1.0m$ and $d = 0.25m$ filled with both a vacuum ($\epsilon_r = 1$) and with lossy dielectric ($\epsilon_r = 4 - j1$). Excellent comparisons are observed for data obtained using the WGM and a finite element-boundary integral (FEBI) technique implemented in [4].

Computed RCS using the WGM and a Fourier transform representation developed in [5] and [6] are shown in Fig. 5 for the case of TE polarization on a deep groove having $W = 8.7m$ and $d = 16m$, filled with $\epsilon_r = 1.5$ lossless dielectric. The 3-D bistatic plot in Fig. 6(a) displays the main specular reflection ridge centered about $\theta = \theta_i$ and the smaller backscattering ridge running along $\theta = -\theta_i$. Strong multiscattering effects within the deep groove are evidenced by undulating

Figure 5. Backscattering 2-D RCS for TE incidence on a deep rectangular groove having $W = 8.7m$ and $d = 16m$ filled with lossless dielectric $(\epsilon_r = 1.5)$. Comparing calculations using Waveguide Modes (WGM) to that from an "Exact" Fourier Transform Approach in [6] at $f = 300$ MHz.

amplitudes along both the specular and backscattering ridges. Introduction of a slight loss $(\epsilon_r = 1.5 - j0.1)$, with skin-depth $\delta = 3.901m$, is considered in Fig. 6(b). This loss effectively absorbs the fields that penetrate the aperture and cancels interactions with the groove sides and bottom, resulting in virtually no backscattered field and a specular ridge primarily due to surface reflection at the aperture.

Further validation trials were performed for a range of aperture and depth dimensions, aspect angles and material constants, with comparisons made between the waveguide mode method and the more analytically rigorous (but more computationally intensive) multi-region cylindrical harmonic approach. An example is presented in Fig. 7, which overlays TE and TM specular and backscatter RCS versus θ_i for a $W = 10.2m$ and $d = 5.1m$ groove loaded with $\epsilon_r = 4$ lossless dielectric. Excellent agreement is shown except for backscattering near grazing incidence of the TE case, where the WGM approximation induces surface wave reflections from the artificial waveguide walls and neglects upper corner diffraction.
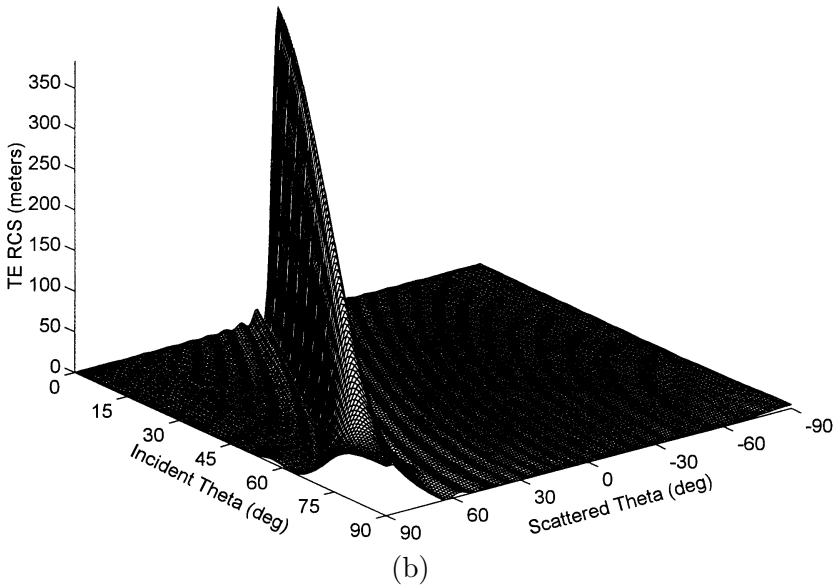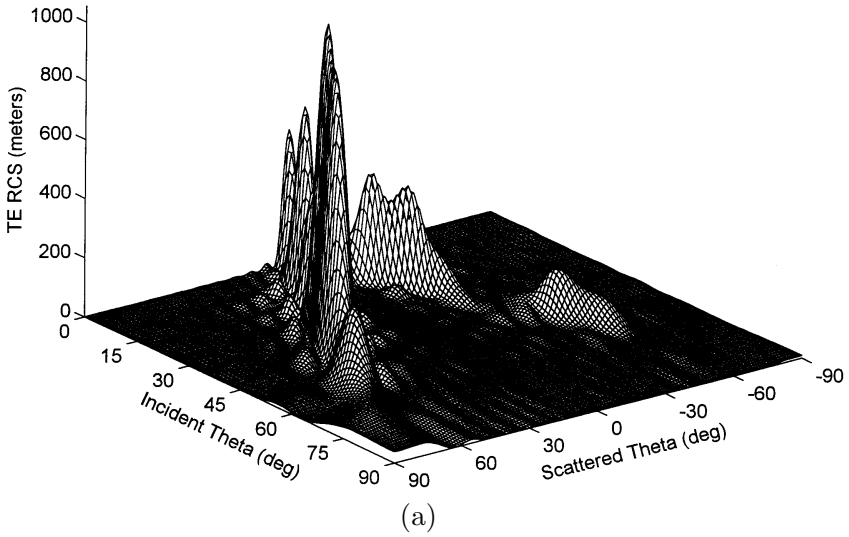
Figure 6. WGM computation of bistatic 2-D RCS (linear scale) for TE incidence on a deep rectangular groove having $W = 8.7m$ and $d = 16m$ for a full range of incident and scattering angles at $f = 300$ MHz. Two cases of material filling: (a) Lossless dielectric $(\epsilon_r = 1.5)$ and (b) Lossy dielectric $(\epsilon_r = 1.5 - j0.1)$.
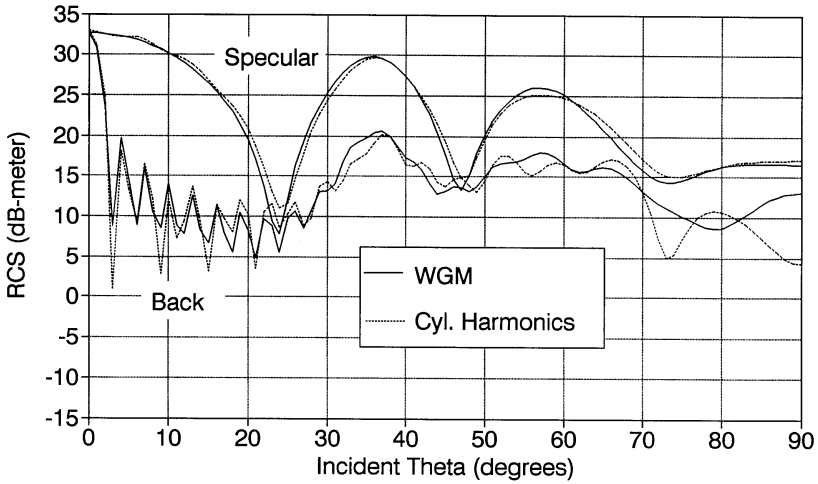
(a)
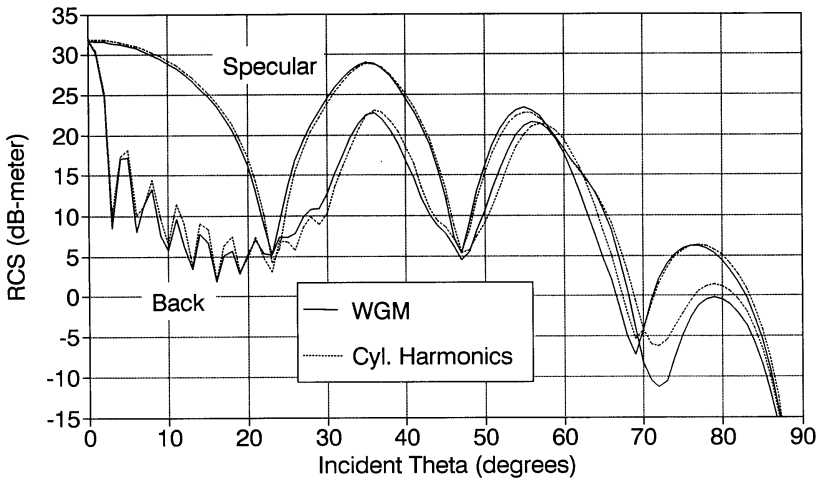
(b)

Figure 7. Specular and backscattered 2-D RCS for a rectangular groove with $W = 10.2m$ and $d = 5.1m$ filled with lossless dielectric $(\epsilon_r = 4, \ \mu_r = 1)$. Comparing TE (a) and TM (b) Case calculations using Waveguide Modes (WGM) to those from a multi-region coupled cylindrical harmonic expansion solution in [7] at $f = 300$ MHz.

Many additional validations for a wide range of groove dimensions and incidence angles have shown that the WGM solution for RCS has converging accuracy not only for electrically large aperture $(W \gg \lambda_0)$ but also for quasi-static low frequencies $(W \ll \lambda_0/2)$. This is exemplified by Fig. 8, which compares WGM and cylindrical harmonic solutions versus frequency for specular and backscattered TM case RCS $(\theta_i = 45°)$ with a free-space filled groove having $W = 1.0m$ and $d = 0.25m$. In this comparison from 10 MHz to 2500 MHz, 522 frequency steps are computed. As a point of reference on efficiency, the WGM approach required 29.27 sec while the cylindrical harmonic solution (which requires matrix system inversions) took 49,550 sec (13.76 hours).
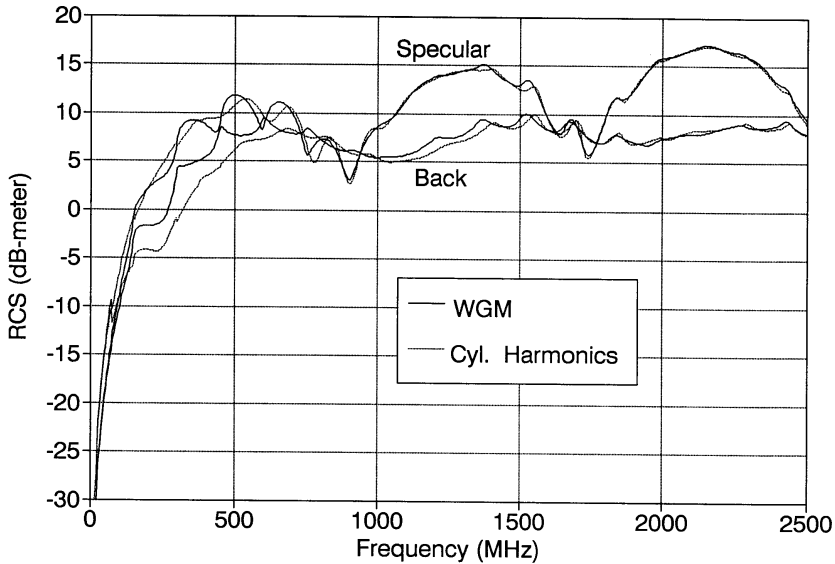
Figure 8 Specular and Backscattered 2-D RCS for $\theta_i = 45°$ TM Incidence on a Free-Space Filled Rectangular Groove with $W = 1.0m$ and $d = 0.35m$. Comparing Frequency Stepping Calculations using Waveguide Modes (WGM) to those from a Multi-Region Coupled Cylindrical Harmonic Expansion.

4. CONCLUSIONS

A simplified approach to scattering by rectangular grooves filled with homogeneous materials has been developed and validated. As a first step in this approximate solution, an exact equivalence to the general groove scattering problem in 3-D is developed which replaces the incident field by a reversed physical optics current in the aperture. The numerical solution is then developed by use of waveguide modes to represent fields in the cavity and in the region above the groove.

The WGM formulation offers a simple alternative which is easy to implement, gives very rapid computation, and has improved accuracy with increasing electrical size. Computational efficiency is important when scattering evaluation is required for numerous cases of electrically large grooves, such as in a statistical analysis for random surfaces. This specific problem, in fact, motivated the development of the WGM.

The WGM can be extended to other groove shapes. For the case of separable coordinates with homogeneous filling, analytic cavity modes can be used. More general groove shapes and even inhomogeneous material filling can be considered through use of sparse matrix finite element solutions.

APPENDIX

A general equivalence principle for 3-D cavity or 2-D trough scattering can be developed by considering the sequence of illustrations in Fig. 9. Figure 9(a) depicts the scattering problem, wherein an arbitrary open cavity in a ground plane containing inhomogeneous material is illuminated by specified sources, $\overline{J}_0$ and $\overline{M}_0$, in the upper region. The total field in the cavity is denoted by $(\overline{E}_1^C, \overline{H}_1^C)$ while the diffraction field $(\overline{E}_1, \overline{H}_1)$ in the upper half-space is composed of the known incident field added to a perturbation field $(\overline{E}_1^S, \overline{H}_1^S)$.

The scattered field that we seek is defined to be $(\overline{E}_1 - \overline{E}_2, \ \overline{H}_1 - \overline{H}_2)$ where $(\overline{E}_2, \overline{H}_2)$ is the upper half-space diffraction field observed in the presence of just the ground plane (without the cavity). To obtain $(\overline{E}_2, \overline{H}_2)$ a hypothetical pec "plug" can be inserted to close the aperture and create a continuous ground plane. The physical optics induced current $\overline{J}_S = 2\hat{n} \times \overline{H}_0^i$ is then excited on the ground plane, including across the pec section covering the cavity aperture.

Based upon the uniqueness concept [10], the fields will remain everywhere the same if the pec plug is removed and the induced current is
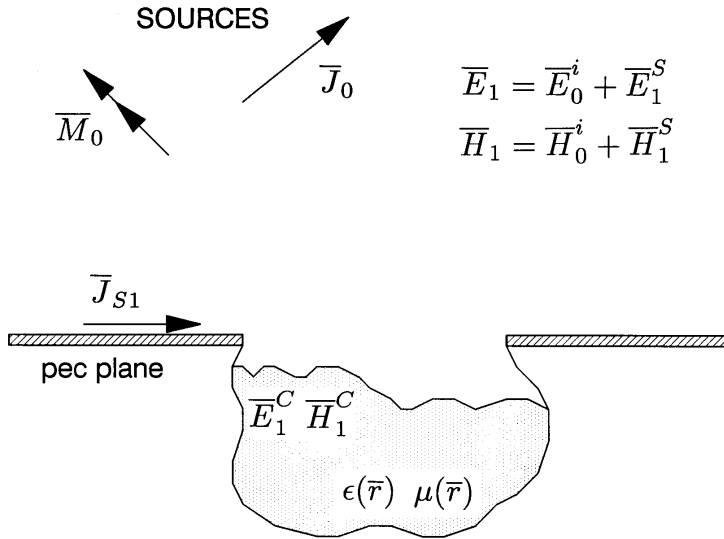
SOURCES

$\overline{J}_0$

$\overline{M}_0$

$\overline{E}_1 = \overline{E}_0^i + \overline{E}_1^S$

$\overline{H}_1 = \overline{H}_0^i + \overline{H}_1^S$

$\overline{J}_{S1}$

pec plane

$\overline{E}_1^C \ \overline{H}_1^C$

$\epsilon(\overline{r}) \ \mu(\overline{r})$

Figure 9(a)

SOURCES

$\overline{J}_0$

$\overline{M}_0$

$\overline{E}_2 = \overline{E}_0^i + \overline{E}_2^S$

$\overline{H}_2 = \overline{H}_0^i + \overline{H}_2^S$

IMPRESSED
APERTURE
CURRENT

$\overline{J}_{S2}$

$\overline{J}_{S3} = 2\hat{n} \times \overline{H}_0^i$

pec plane

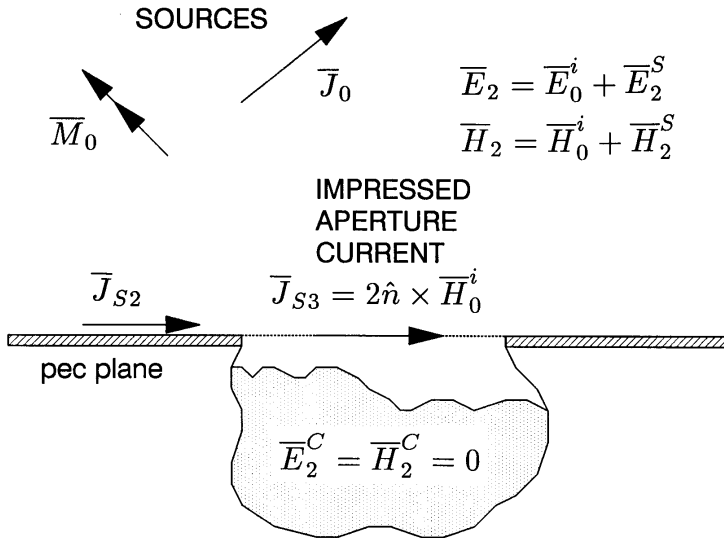$\overline{E}_2^C = \overline{H}_2^C = 0$

Figure 9(b)

Figure 9. Cavity Scattering Equivalence Theorem Development: (a) Original Scattering Problem; (b) Field Equivalence for PEC Covered Aperture.

SOURCES
REMOVED

$$\overline{E}_3 = \overline{E}_1 - \overline{E}_2 = \overline{E}^S$$

$$\overline{H}_3 = \overline{H}_1 - \overline{H}_2 = \overline{H}^S$$

IMPRESSED
APERTURE
CURRENT

$$-\overline{J}_{S3}$$

pec plane

$$\overline{E}_1^C \ \overline{H}_1^C$$
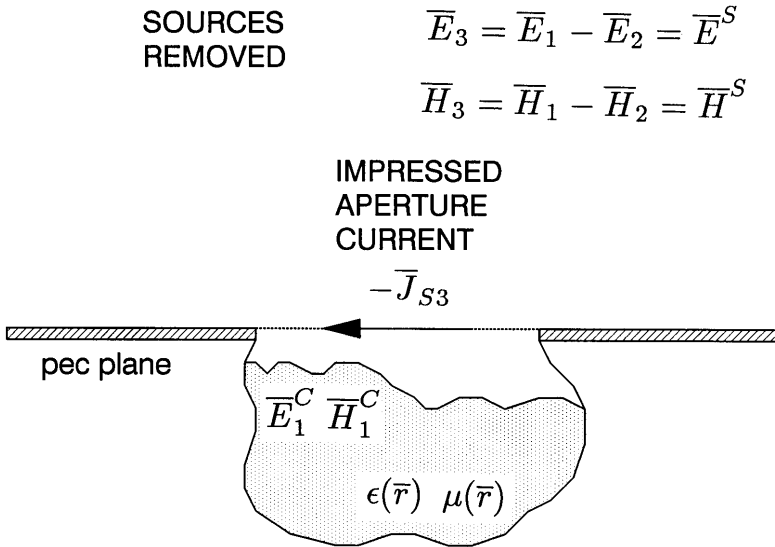
$$\epsilon(\overline{r}) \ \ \mu(\overline{r})$$

Figure 9(c)

Figure 9. Cavity Scattering Equivalence Theorem Development: (c) Scattered Field Equivalence Found From Superposition of (a) Minus (b).

replaced by an identical impressed sheet current covering the aperture. This situation is shown in Fig. 9(b), where the impressed current $\overline{J}_{S3}$ equals the physical optics $\overline{J}_S$ over the aperture while the induced $\overline{J}_{S2}$ equals $\overline{J}_S$ over the remainder of the ground plane. $\overline{J}_{S2}$ is induced by both the original sources, $\overline{J}_0$ and $\overline{M}_0$, and $\overline{J}_{S3}$.

Applying superposition, it is apparent that generation of the scattered field can be accomplished by impressed sources which are the difference of those in Figs. 9(a) and 9(b). This shown in Fig. 9(c). Thus, an impressed $-\overline{J}_{S3} = -2\hat{n} \times \hat{H}_0^i$ covering the aperture and radiating in the presence of the cavity generates the scattered field being sought in the upper half-space while producing the original cavity field.

REFERENCES

1. Butler, C. M., Y. Rahmat-Sammi, and R. Mittra, "Electromagnetic penetration through apertures in conducting surfaces," *IEEE Trans. Antennas Propagat.,* Vol. AP–26, No. 1, 82–93, January 1978.

2. Barkeshli, K., and J. L. Volakis, "TE scattering by a two-dimensional groove in a ground plane using higher order boundary conditions," *IEEE Trans. Antennas Propagat.,* Vol. AP–38, No. 9, 1421–1428, September 1990.

3. Whites, K. W., E. Michielssen, and R. Mittra, "Approximating the scattering by a material-filled 2-D trough in an infinite plane using the impedance boundary condition," *IEEE Trans. Antennas Propagat.,* Vol. AP–41, No. 2, 146–153, February 1993.

4. Lin, J. M., and J. L. Volakis, "TM scattering by an inhomogeneously filled aperture in a thick conducting plane," *IEEE Proceedings.,* Vol. 137, Pt. H, 153–159, June 1990.

5. Park, T. J., H. J. Eom, and K. Yoshitomi, "An analytical solution for transverse- magnetic scattering from a rectangular channel in a conducting plane," *J. Appl. Phys.,* Vol. 73, No. 7, 357–3573, 1993.

6. Park, T. J., H. J. Eom, and K. Yoshitomi, "An analysis of transverse electric scattering from a rectangular channel in a conducting plane," *Radio Science,* Vol. 28, 663–673, Sept. – Oct. 1993.

7. Morgan, M. A., "Scattering computations from multi-region cylindrical objects," *Proceedings of the Ninth Annual Review of Progress in Applied Computational Electromagnetics,* Monterey, CA, March 1993.

8. Collin, R. E., *Field Theory of Guided Waves,* 2nd edition, Chapter 6, New York: IEEE Press, 1991.

9. Collin, R. E., and F. J. Zucker, *Antenna Theory, Part 1,* Chapter 3, New York: McGraw-Hill, 1969.

10. Harrington, R. F., *Time-Harmonic Electromagnetic Fields,* Chapter 3, New York: McGraw-Hill, 1961.